Article

Virus Mimetic Poly (I:C)-primed Airway Exosomes Enter Brain and Induce Mitochondrial Reactive Oxygen Species in Microglia

Deimantė Kulakauskienė[1,2], Deimantė Narauskaitė[1], Dovydas Gečys[1,3], Otilija Juknaitė[1], Lina Jankauskaitė[1,4,5], Aistė Masaitytė[6], Jurgita Šventoraitienė[6], Hermanas Inokaitis[6], Zoja Miknienė[7], Ilona Sadauskienė[8], Zbigniev Balion[1,9], Ramunė Morkūnienė[2], Neringa Paužienė[6], Dainius H. Pauža[6], Aistė Jekabsone[1,10] *

[1] Institute of Pharmaceutical Technologies, Faculty of Pharmacy, Lithuanian University of Health Sciences; D.K. - deimante.kulakauskiene@lsmu.lt; D.N.- deimante.narauskaite@lsmu.lt; D.G. - dovydas.gecys@lsmuni.lt; O.J. - otilija.juknaite97@gmail.com; L.J. - lina.jankauskaite@lsmuni.lt; Z.B. - zbigniev.balion@lsmuni.lt; A.J. - aiste.jekabsone@lsmuni.lt

[2] Department of Drug Chemistry, Faculty of Pharmacy, Lithuanian University of Health Sciences; R.M. - ramune.morkuniene@lsmuni.lt

[3] Laboratory of Molecular Cardiology, Institute of Cardiology, Lithuanian University of Health Sciences;

[4] Institute of Physiology and Pharmacology, Faculty of Medicine, Lithuanian University of Health Sciences;

[5] Clinical Department of Pediatrics, Faculty of Medicine, Lithuanian University of Health Sciences;

[6] Institute of Anatomy, Faculty of Medicine, Lithuanian University of Health Sciences; A.M. - a.masaityte@gmail.com; J.Š. - jurgita.sventoraitiene@lsmuni.lt; H.I. - hermanas.inokaitis@lsmuni.lt; N.P. - neringa.pauziene@lsmuni.lt; D.H.P. - dainius.pauza@lsmuni.lt

[7] Large Animal Clinic, Faculty of Veterinary Medicine; Lithuanian University of Health Sciences; zoja.mikniene@lsmuni.lt

[8] Laboratory of Molecular Neurobiology, Neuroscience Institute, Lithuanian University of Health Sciences; Ilona.sadauskiene@lsmuni.lt

[9] Laboratory of Biochemistry, Neuroscience Institute, Lithuanian University of Health Sciences;

[10] Laboratory of Preclinical Drug Investigation, Institute of Cardiology, Lithuanian University of Health Sciences.

* Correspondence: aiste.jekabsone@lsmuni.lt; Tel.: +370 675 94455

Simple Summary: Upper respiratory tract viral infections are among the most common diseases. The blood-brain barrier protects the brain from direct invasion of pathogens. However, the cells share their content with other cells in small nanovesicles called exosomes that can travel long distances and cross biological barriers. Virus-infected cell exosomes might transmit inflammatory signals or even viral particles to other cells. If they would carry such signals or particles to the central nervous system, it might cause neuroinflammation. However, the migration and impact of virus-primed airway exosomes on the brain have not been studied yet. Therefore, the study aimed to track airway exosomes from the respiratory tract to the brain and determine how infection-primed exosomes affect microglia - the cells responsible for immune response in the brain. The study revealed that airway cell exosomes enter the brain within an hour and gather in microglia. Interestingly, many airway exosomes were found in the hippocampus, the region most affected by Alzheimer's disease. Moreover, exosomes from virus-infected airway cells stimulated reactive oxygen species in microglia. The elevated level of reactive oxygen species is one of the features of microglial inflammatory activation. Thus, airway cells indeed might communicate inflammatory information to the brain during viral infection.

Abstract: Viral infections induce exosomes containing viral material and inflammatory factors. During respiratory tract infection, exosomes can easily cross the blood-brain barrier and transmit the inflammatory signal to the brain; however, such a hypothesis has no experimental evidence. The study investigated whether exosomes from virus mimetic poly (I:C)-primed airway cells enter the brain and interact with brain immune cells microglia. Airway cells were isolated from Wistar rats and BALB/c mice; microglial cell cultures - from Wistar rats. Exosomes from poly (I:C)-stimulated airway cell culture medium were isolated by precipitation, visualised by transmission electron microscopy, and evaluated by nanoparticle analyser; exosomal markers CD81 and CD9 were

determined by ELISA. For *in vitro* and *in vivo* tracking, exosomes were loaded with Alexa Fluor 555-labelled RNA. Intracellular reactive oxygen species (ROS) were evaluated by DCFDA fluorescence and mitochondrial superoxide - by MitoSOX. The exosomes from poly (I:C)-primed airway cells entered the brain within an hour after intranasal introduction, were internalised by microglia, and induced intracellular and intramitochondrial ROS production. There was no ROS increase in microglial cells was after treatment with exosomes from airway cells untreated with poly (I:C). The data indicate that virus-primed airway cell exosomes might enter the brain and induce the activation of microglial cells.

Keywords: airway cell exosomes; viral infection; microglia; mitochondria; reactive oxygen species.

1. Introduction

The upper respiratory tract is considered a gateway for viruses to enter the human body. Approximately 90% of the upper airway tract infections are caused by viruses [1], and over 200 different viruses have been isolated from the human upper respiratory tract [2]. Generally, respiratory viruses, such as rhinoviruses, influenza, adenoviruses, enteroviruses, does not spread to the distant tissues; however, accumulating evidence shows that viral material carried by extracellular vesicles (EVs) originating from infected cells might induce cellular alterations outside of the respiratory tract [3–5].

Exosomes are 30-150 nm diameter extracellular vesicles essential for intercellular communication [6]. They are secreted by almost every cell type and present in various body fluids, including urine, blood, breast milk, and saliva [7]. Exosomes contain different bioactive molecules such as proteins, lipids and several RNA species [8]. Studies have shown that exosomal cargo depends on the physiological state of the parental cell [3,9,10]. It was observed that exosome content alternates in response to viral infection and that exosomes isolated from infected cells were able to activate innate immune response [3]. Several studies have shown that viral material transported by EVs can induce immune response [11], viral replication [12], cell apoptosis, cytokine release suppression [13,14], as well as contribute to NLRP3 inflammasome and IL-1β production [15]. Additionally, it was well established that exosomes can effectively cross the blood-brain barrier and carry endogenous material to the brain from the peripheral circulatory system [16,17].

One of the most plausible exosome recipients in the brain are microglial cells. Microglia and non-parenchymal macrophages in the brain are mononuclear phagocytes that are essential in brain homeostasis. Microglia constitute 5–10% of total brain cells and are the only true CNS parenchymal macrophages that can interact with neurons, astrocytes and oligodendrocytes [18,19]. Microglia are involved in synaptic plasticity by synaptic pruning in the developing and adult brain; they also phagocytose dying, dead, and sometimes healthy cells [20–22]. Additionally, microglia respond to an infection or brain damage by transforming into an active inflammatory phenotype and protecting the brain from pathogens. However, prolonged microglial activation might lead to neurodegenerative disease development [23]. Recent evidence indicates that peripheral infections can stimulate an immune response in the brain, causing irreversible genetic and epigenetic changes in brain immune cells leading to the formation of immune memory [24]. Antiviral immune response and immune memory formation are related to rearrangements in mitochondrial network and dynamics and involve reactive oxygen species (ROS) signalling [25]. Exosomes might carry viral particles and/or inflammatory molecules. One might speculate that exosomes produced during frequent recurrent viral respiratory infections might cause microglia activation and maintenance of immune reactivity in the brain. However, such a hypothesis has no experimental evidence yet. This study investigates whether exosomes from virus mimetic TLR-3 agonist poly (I:C)-affected airway cell exosomes can enter the brain and how they interact with brain immune cells microglia.

2. Materials and Methods

2.1. Experimental design

The experimental design of the study is represented in Figure 1. First of all, airway cells were isolated from laboratory rodent lungs, cultivated and primed with poly (I:C). Then, exosomes were isolated, characterised and prepared for *in vivo* intranasal and *in vitro* cell culture introduction. In parallel, primary microglial culture was prepared. Next, the poly (I:C)-treated and untreated airway exosomes were introduced to cultivated microglia, and the cultures were monitored for exosome internalisation and intracellular plus intramitochondrial ROS production. In addition, stained airway cell exosomes were intranasally introduced to laboratory mice, and exosome localisation in immunostained microglial cells in the brain cryosections was monitored after 1, 2, 3, and 5 hours.
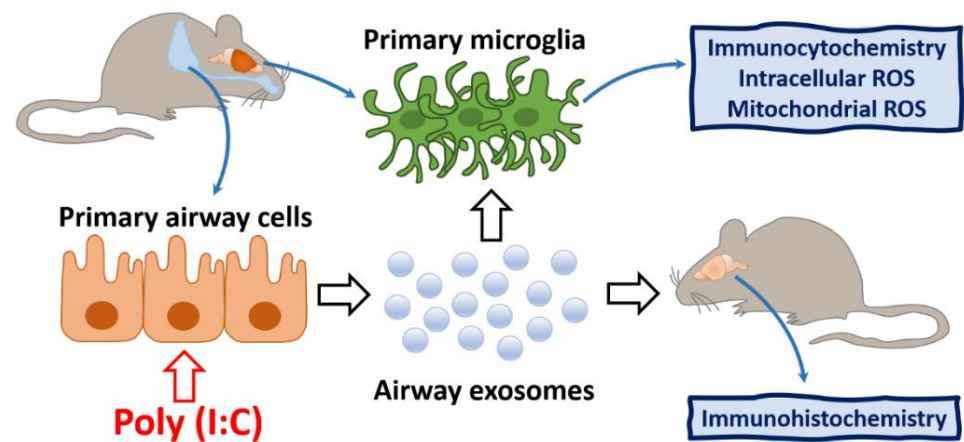

Figure 1. The experimental design of the study. Primary airway cells of rodent origin were treated with poly (I:C), and their exosomes were applied on microglial cell cultures and intranasally to mice. Microglial cells *in vitro* and *in vivo* were investigated for exosome internalisation, and cultured microglia were analysed for intracellular and intramitochondrial ROS production.

2.2. Culture of primary airway cells

Primary airway cells were prepared from 6–7-day-old Wistar rats for *in vitro* studies, and primary mouse airway cells for *in vivo* studies were made from 9-11 weeks old Balb/c mice for *in vivo* experiments. All experimental procedures were performed according to the Republic of Lithuania Law on the Care, Keeping and Use of Animals. The mice were maintained and handled at the Lithuanian University of Health Sciences animal house in agreement with the ARRIVE guidelines.

For isolation of airway cells, the animals were sacrificed by cervical dislocation. The trachea and lungs were exposed and removed from the thorax. After, the heart, trachea and large bronchi were removed. The remaining lung tissue was rinsed twice with PBS, further processed in DMEM and manually homogenised with the sharp scissors. Pieces of lung tissue were transferred into a conical tube, and 5ml of digestion medium (DMEM, 1% trypsin) was added. Then, the tube with the tissue was incubated for up to 30 min at 37°C by gentle rocking every 15min. After incubation, the digestion process was inactivated with the DMEM and 10% FBS. Further, all tissue pieces were filtered through the 70-μm cell strainer to obtain a single-cell suspension. The strainer was discarded, and the tube was further centrifuged at 1200 rpm for 10min at 4°C. The supernatant was removed, cells were suspended in the, counted, seeded, and cultivated in a T-75 flask with a growth medium (DMEM with GlutaMAX™, 10% FBS and 1%, or 10000 IU/mL, penicillin-

streptomycin solution). After 24h, the supernatant was removed and centrifuged again. All adherent cells (fibroblasts) were discarded. The centrifuged cells were then seeded and cultivated in a T-75 flask in the growth medium until further experiments.

2.3. Cultures of primary mixed glia and pure microglia

Mixed glial and pure microglial cultures were prepared from 6–7-day-old Wistar rat pups, as described in [26], with minor modifications. All animal care and procedures were performed according to the Republic of Lithuania Law on the Care, Keeping and Use of Animals following ARRIVE guidelines. Briefly, after decapitation, cerebral cortices were separated from the remaining parts of the brain and placed in Petri dishes containing PBS, glucose (13 mM), and penicillin-streptomycin solution (10000 IU/mL – 10000 μg/mL). After removing the meninges, the cortical tissues were cut and transferred to the centrifugal tube with preheated (37°C) Versene (Gibco™, USA, 1:50000) solution and incubated for 10 min in 37°C with gentle agitation. After incubation, the solution was tittered and centrifuged at 290 x g at room temperature. The pellet was resuspended in cell growth media (DMEM with GlutaMAX™ and 10% FBS). The resuspended cells were passed through 40 μm mesh, transferred to poly-L-lysine coated T-75 flasks and cultivated for 13 days replacing growth medium every 5th day. Microglial cells were isolated by gently shaking the flask for 5 min on an orbital shaker. Media with detached microglial cells were collected and pelleted by centrifugation at 290 g for 5 min. Microglial cells were further cultivated in T-75 flasks using DMEM-GlutaMAX™ growth medium supplemented with 10% FBS and 1% penicillin-streptomycin solution.

2.4. Exosome isolation

Rat and mouse airway cells were cultured in 75 cm² flasks, in 75 cm2 flasks, in DMEM-GlutaMAX™ medium with 10% FBS, 25 mM HEPES, and 1% penicillin-streptomycin solution at 37°C. After reaching 70-80% confluency, the growth medium was replaced to FBS-depleted composition to avoid contamination with EVs that are present in the serum. The cells were treated with 1 μg/mL poly (I:C) for 1 hour and then incubated for 24 hours in a serum-free medium without poly (I:C). After collection, the cell-conditioned medium was passed through 0.22 μm PVDF filters. Exosomes were isolated using Total Exosome Isolation Reagent (Invitrogen) according to the manufacturer's manual. Briefly, conditioned media were mixed with the reagent at a ratio of 2:1. The mixture was incubated at 4°C for 16 hours and centrifuged at 10000 x g for 1 hour at 4°C. The pellets were resuspended in 250 μl of PBS, aliquoted and stored at -80°C for further use.

2.5. Exosome characterisation

The amount of total protein in exosome samples was determined by Bradford assay (Sigma-Aldrich, Germany) measuring absorbtion of λ=595 nm light in a Tecan Infinite 200 PRO plate reader. The exosomal markers tetraspanins CD63 and CD9 were quantified by ELISA kits (Abbexa CD63 ELISA Kit and Abbexa MRP1 ELISA Kit) according to the manufacturer's instructions.

The nanoparticle size distribution in isolated exosome preparations was determined by dynamic light scattering (ZetaSizer Nano ZS, Malvern PANalytical, UK). In short, 50 μl of exosome preparation was homogenised for 5 minutes using 30G needle. Ten microliters of exosome preparation were mixed with 1990 μl of PBS in analytical cuvettes, monitored in the analyser, and the data were processed by ZetaSizer Nano software.

Exosome imaging was performed by transmission electron microscopy. Isolated exosomes were homogenised for 5 min with 30G needle and mixed with 4% paraformaldehyde at the ratio of 1:1. This solution was applied on carbon-coated Formvar copper meshes FCFT200-Cu-50 200 MESH (Sigma-Aldrich, Germany). The meshes were fixed in 1.7% glutaraldehyde solution for 5 min, washed twice in deionised water for 2 min and stained with 2% uranyl acetate for 2 min. After staining, the meshes were incubated with freshly prepared 2.25% methylcellulose and 2% uranyl acetate in a v/v ratio of 4:1 for 10

min on an ice table. Prepared meshes were carefully dried on filter paper for 10 to 15 min and visualised using a transmission electron microscope Tecnai BioTwin Spirit G2 (FEI, Eindhoven, the Netherlands) on 80 kV voltage. Electron microscope images were taken with a bottom-mounted 16 MP TEM CCD camera Eagle 4K employing TIA (FEI, Eindhoven, the Netherlands).

2.6. Exosome labelling for in vitro and in vivo tracking

Exosomes were labelled with Alexa Fluor 555 dye (BLOCK-it Alexa Fluor Red Fluorescent Control, Invitrogen) by lipofection (RNAiMAX, Invitrogen). Briefly, a mixture of 0.2 µM of Alexa Fluor 555 dye was mixed with 3 µl of RNAiMAX reagent in 100 µl of the Opti-MEM™ medium (Thermo FischerScientific) and incubated for 5 min at room temperature. Exosome preparation (1 mg/mL of total protein) was added into lipofection mixture and incubated at 37°C for one hour. After incubation, unincorporated dye and residual micelles were removed using Exosome spin columns (Invitrogen). Labelled exosomes were concentrated using 100K Amicon® Ultra centrifugal filters (Millipore) and used for internalisation and tracking analysis.

2.7. Intranasal in vivo administration of airway exosomes

All experimental procedures were performed on 4-month-old Balb/c mice according to the Law of the Republic of Lithuanian Animal Welfare and Protection (License of the State Food and Veterinary Service for working with laboratory animals No. G2-96). The mice were maintained and handled at the Lithuanian University of Health Sciences animal house in agreement with the ARRIVE guidelines. Before the intranasal administration of fluorescently labelled exosomes, each nostril was treated with 100U hyaluronidase dissolved in 5 µl PBS to increase the permeability of the mucus. After 30 min, 25 µl of exosome solution containing 30 µg of exosomal protein was introduced to each nostril (60 µg per mouse). The solution was administered gradually in 5 µl portions followed by a 5 min interval and alternating the nostrils. After 1, 2, 3, and 5 hours, the mice were anaesthetised and sacrificed, and the brains were further processed for immunohistochemical analysis.

2.8. In vitro exosome tracking and viability assessment

For exosome uptake *in vitro* evaluation, Alexa Fluor 555-labelled exosome solution containing 0,5 mg/mL of total protein in PBS was applied on mixed glial and microglial cultures. After 20 min of incubation, Hoechst33342 (6 µg/mL, Thermo Fisher Scientific) was added to the incubation medium for visualisation of nuclei and isolectin GS-IB$_4$ from *Griffonia simplificolia*, Alexa Fluor® 488 conjugate (10 ng/mL, Molecular Probes) for staining microglial with microglial and mixed glial using fluorescence microscope Zeiss Axio Observer.Z1 (Carl Zeiss, Jena, Germany).

The viability of microglial cells in pure microglial cultures after exosome uptake was assessed by double nuclear staining with fluorescent dyes Hoechst33342 (6 µg/mL) and propidium iodide (3 µg/mL) for 10 min and imaging in a fluorescent microscope Olympus IX71 (Olympus Corporation, Tokyo, Japan). The images were taken by a 01-Exi-AQA-R-F-M-14-C camera (QImaging, Surrey, Canada) and the image analysis was performed by the ImageJ software.

2.9. Immunohistochemistry of brain tissue

Animal brains were rapidly removed, immediately washed in PBS and embedded in 4% paraformaldehyde solution for 30 min. Afterwards, the brains were transferred to 25 % sucrose and kept there for 24 h at 4 °C. Then the tissue was frozen in liquid nitrogen and stored at −80 °C until further processing. Next, serial coronal sections (20 µm thick) containing the substantia nigra were cut at −23 °C using a cryostat (HM 560 Microm, Walldorf , Germany). The sections were mounted on glass slides (Plus, Menzel Glaser), and the slides

were allowed for complete dehydration in the cryostat chamber for 10 min. The slides were washed with PBS solution (3 x 10 min) and subjected to 0.5% Triton X-100 permeabilisation for 40-60 minutes at room temperature in a dark, humid environment. The slides were then washed with PBS (3 x 10 min) and incubated overnight with 1 µg/mL primary rabbit monoclonal antibodies against microglial transmembrane protein TMEM119 (RRID:AB_2800343, ab209064, Abcam) overnight at 4°C. After 3 x 10 min washing with PBS, the slides were incubated with AlexaFluor®488 conjugated chicken anti-rabbit IgG (Thermo Fisher Scientific) secondary antibodies diluted in PBS 1:200 for 2 hours at room temperature, in a dark and humid environment. The slides were then rewashed with PBS (3 x 10 min) and coated with anti-fading oil (Vectashield, Vector Laboratories), the edges varnished with colourless nail polish. For negative control, only PBS solution was added instead of primary antibodies, followed by secondary antibodies. The stained tissue was visualised by laser scanning confocal microscope: Zeiss Axio Observer LSM 700 (Carl Zeiss Microimaging Inc., Jena, Germany).

2.10. Evaluation of intracellular and intramitochondrial ROS

Cytoplasmic and intramitochondrial ROS were evaluated as described in [27]. Briefly, the 2′, 7'-dichlorofluorescein diacetate (DCFDA, Invitrogen) was used to assess the formation of intracellular ROS in microglia. Microglial cells were seeded in 96-well plates (50 000 / well) and cultivated for 24 h. After incubation, cells were treated with poly (I:C)-primed and not primed airway cell exosomes (10 µg/ml of total protein) for 16–18 h. After incubation, all cells were washed with Hank's Balanced Salt Solution (HBSS, Gibco). Following washes, cells were stained with 10 µM DCFDA for 30 min at 37°C, repeatedly washed with HBSS and visualised using Olympus IX2-ILL100 fluorescence microscope (Olympus, Japan). To evaluate mitochondrial superoxide, the cells were grown in clear 96-well plates the same way as for cytoplasmic ROS assessment. The cells were 3x washed with HBSS and incubated with 2 µM MitoSoxTM Red (Thermo Fisher Scientific) in HBSS at 37 °C in the dark for 15 min. The images were taken by fluorescent microscope Zeiss Axio Observer.Z1, and fluorescence intensity was evaluated by ImageJ software.

2.11. Statistical analysis

Statistical analysis was performed using Sigma Plot v12.5 software. The means of the experimental data are presented with standard errors. Statistical comparisons of the two groups were performed using Student's t-test. Multiple groups were compared using and one-way analysis of variance (ONE WAY ANOVA) with Bonferroni statistical criterion. Differences between means were considered statistically significant at $p < 0.05$.

3. Results

3.1. Identification and characterisation of airway cell exosomes

At first, exosomes isolated from poly (I:C)-primed and not primed rat airway cell-conditioned medium were evaluated for morphology by transmission electron microscopy (TEM). The samples contained vesicles of approximately 10 – 190 nm in diameter (Figure 2a,b).
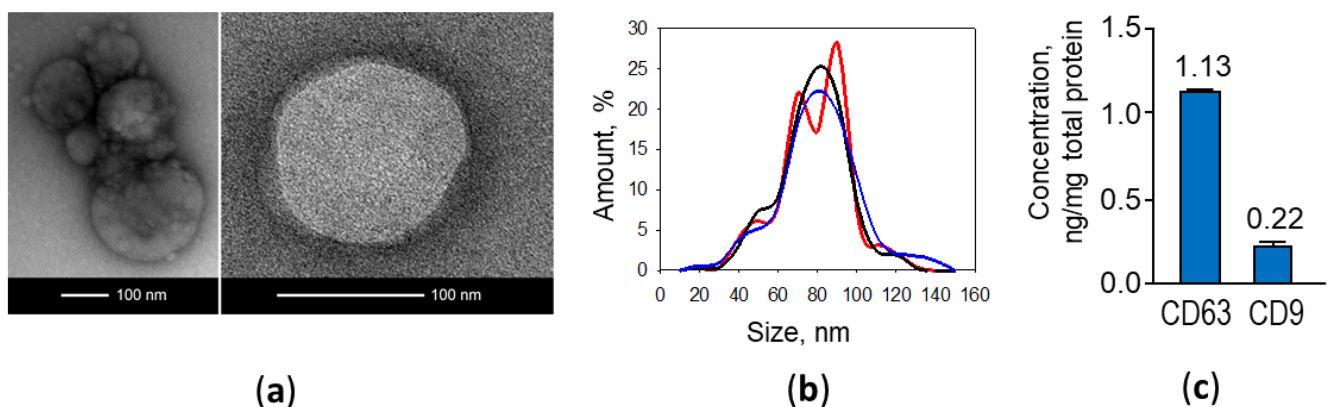
Figure 2. Poly (I:C)-treated rat airway cell exosome morphology, particle size distribution and specific markers. Representative transmission electron microscopy images (**a**), dynamic ligh scattering nanoparticle analysis data of three samples (**b**) and tetraspanin CD63 and CD9 content per total exosome preparation protein determined by ELISA.

The dynamic light scattering analysis revealed that the particle diameter in exosome samples ranged from 10 to 160 nm, and 98 per cent of the particles in the samples were in the range of 30-150 nm, which is characteristic for exosomes (Figure 2c). Next, exosome preparations were ELISA-tested for common exosomal markers, tetraspanins CD9 and CD63. The analysis confirmed both markers present in the samples; however, CD63 was found about five times more than CD9 (Figure 2d). Similar characteristics were found by examining exosome preparations from mice airway cell cultures (Figure A1). There were no detectable differences in morphology, size distribution and CD63/CD9 presence found between poly (I:C)-primed and not primed airway cell exosomes (data not shown).

3.2. Poly (I:C)-primed airway exosome tracking in brain and microglia

For blood-brain barrier penetration monitoring, Alexa Fluor-555 (AF555) labelled exosomes from poly (I:C)-primed airway cells were applied on microglial cell cultures and introduced intranasally to mice. Red fluorescence became visible in the brain already 1 hour after treatment, and later (after 3 and 5 hours), the fluorescence spots became more extensive (Figure 3a). Some of them resembled cell body shape suggesting that exosomes were internalised by specific cells at this time point. Interestingly, some brain regions, such as the hippocampal pyramidal neuron layer, were more prone to collect exosomes (Figure 3b). There was no red staining visible in brain slices from mice that did not receive exosome treatment (0h image in Fig. 3a).

Next, the brain slices were immunostained for TMEM19 to determine if the exosomes were internalised by microglial cells. The staining revealed that most exosomes colocalised with microglial cell bodies or their processes (Figure 4a), indicating that microglia indeed uptake exosomes after entering the brain. *In vitro* experiments on cultivated rat pure microglia and mixed glia where microglial cells grow on top of astrocytes confirmed that microglia cells internalise exosomes more rapidly than others. All exosomes were entirely relocated to microglial cells 30 minutes after addition to the culture medium in both pure microglial and mixed glial cultures (Figure 4b). The exosomes looked like they collected into cytoplasmic vesicles suggesting that the uptake pathway was either endocytosis, phagocytosis, or micropinocytosis. Such exosome internalisation did not affect the viability of microglial cells; double nuclear fluorescent staining with Hoechst33342 and propidium iodide revealed no significant difference in viable cell number between exosome-treated and untreated, as well as between poly (I:C)-primed and not primed airway exosome-treated microglial cultures; the percentage of viable cells in all cultures were above 98% (Figure A2).
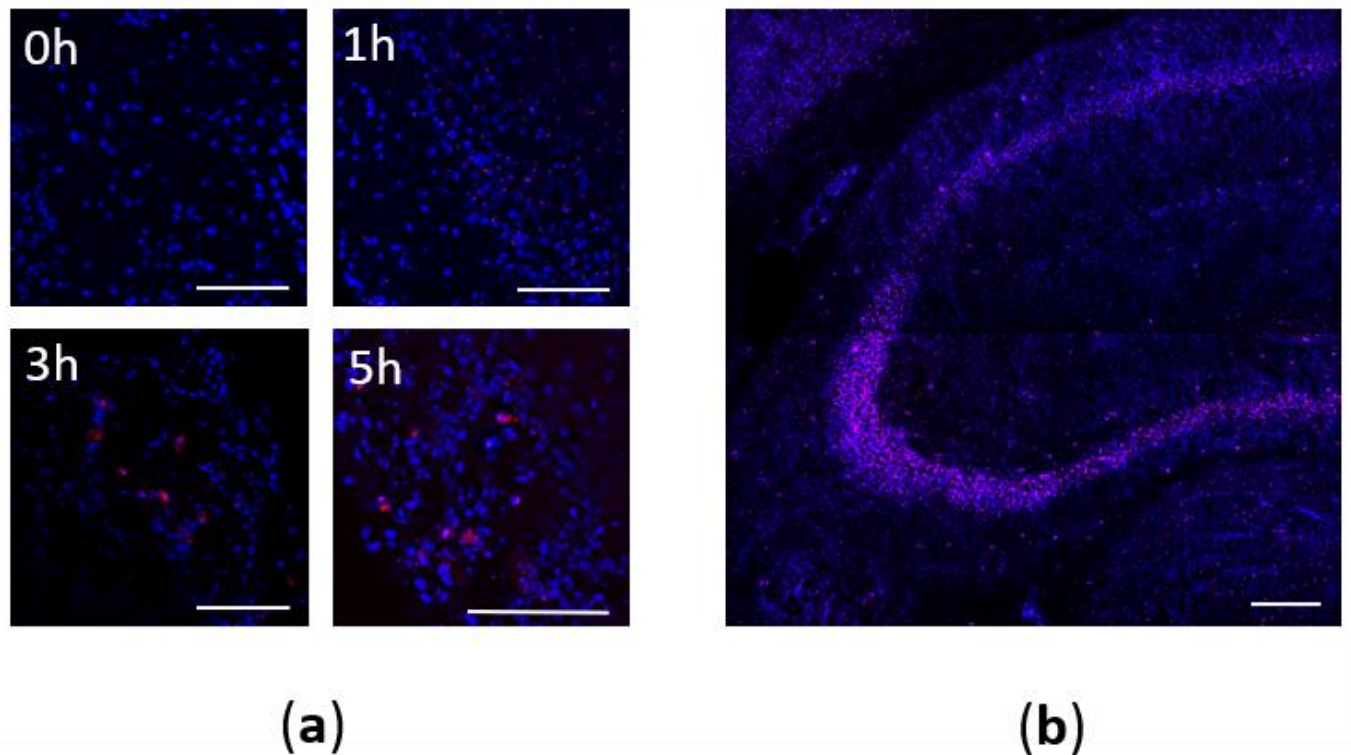
Figure 3. Exosomes from poly (I:C)-treated airway cells in mouse brain sections after 0, 1, 3, and 5 hours following intranasal introduction (**a**). In (**b**) – exosomes in mouse hippocampus 1 hour after introduction. Exosomes loaded with RNR-conjugated AF555 are red, and nuclei are stained blue with DAPI. Scale bar 100 μm.
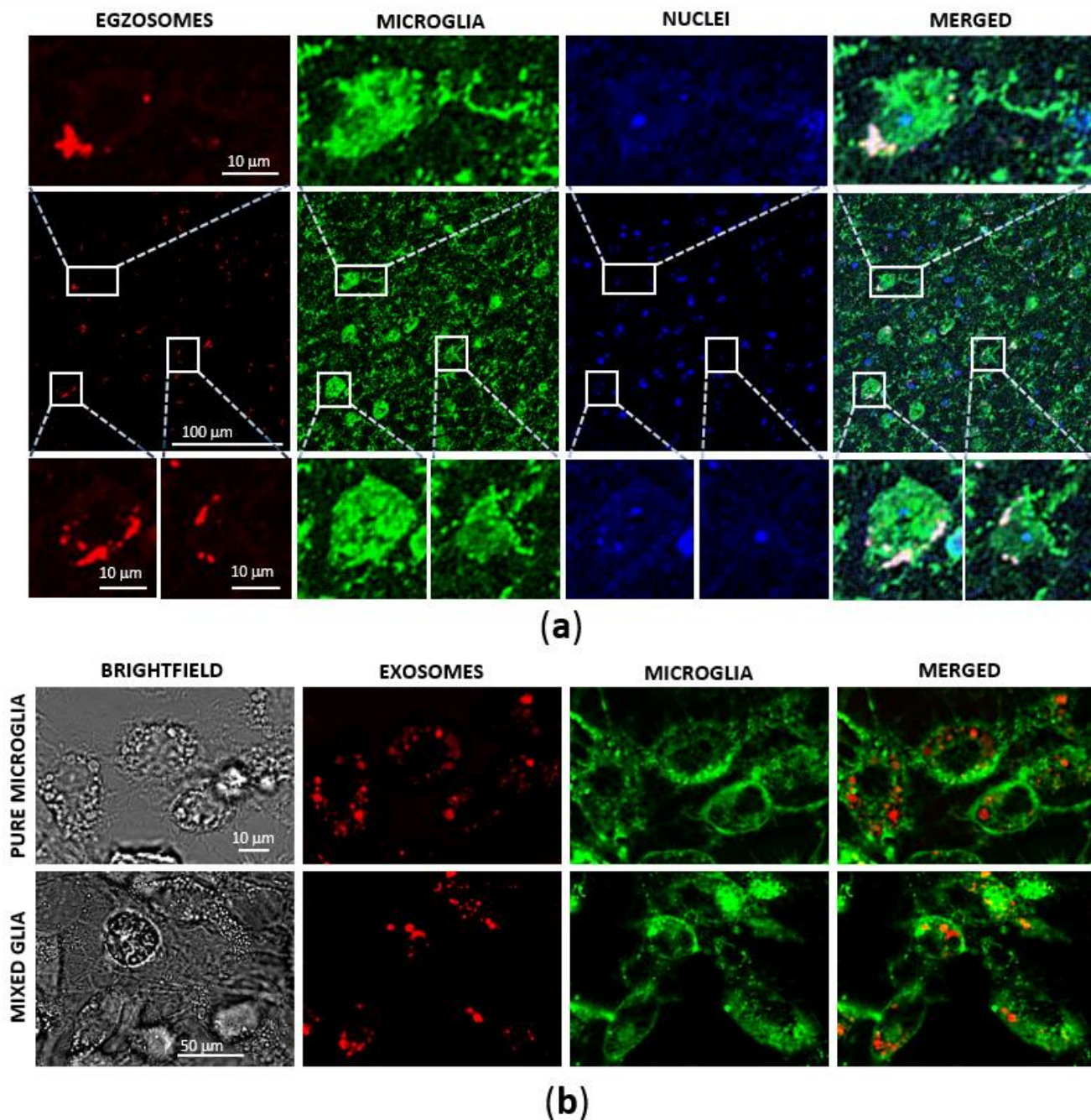
Figure 4. Poly (I:C)-treated airway cell exosome internalisation by microglia in mouse brain 2 hours after intranasal introduction (**a**) and in cultivated rat glial cultures 30 min after treatment (**b**). Exosomes loaded with RNR-conjugated AF555 are red, nuclei are stained blue with DAPI (in **a**) or Hoechst33342 (in **b**). Microglial cells are green visualised by immunostaining against TMEM119 (in **a**) or affinity staining with isolectin B$_4$ (in **b**).

3.3. Poly (I:C)-primed airway cell exosome impact on ROS formation in microglia

Mitochondrial and cytoplasmic ROS act upstream of the inflammatory cascade during viral infection and play a crucial role in immune memory formation [28–30]. To determine whether poly (I:C)-primed airway exosomes affect mitochondrial and cytoplasmic ROS production, microglial cells were incubated with the exosomes for 16 −18 hours, loaded with either MitoSOX™ or DCFDA and monitored under a fluorescent microscope. Both visual monitoring and quantitative evaluation of the micrographs revealed that poly (I:C)-stimulated airway cell exosomes significantly increased the

formation of mitochondrial ROS in microglial cells (Figure 5a). After 24 hours, the MitoSOX™ fluorescence intensity was by 31% higher compared to the samples treated with untreated airway cell exosomes. Moreover, the increased level of mitochondrial ROS in poly (I:C)-primed airway cell exosome-treated samples remained even after 48 hours after the treatment. Additionally, exosomes from poly (I:C)-primed airway cells significantly increased the formation of cytoplasmic ROS in microglia; the DCFDA fluorescence level after 24 hours post-treatment rose by 14% (Figure 5b). There was no significant difference in MitoSOX™ and DCFDA fluorescence intensity between untreated control (100%) and samples treated with exosomes from airway cells unaffected by poly (I:C).
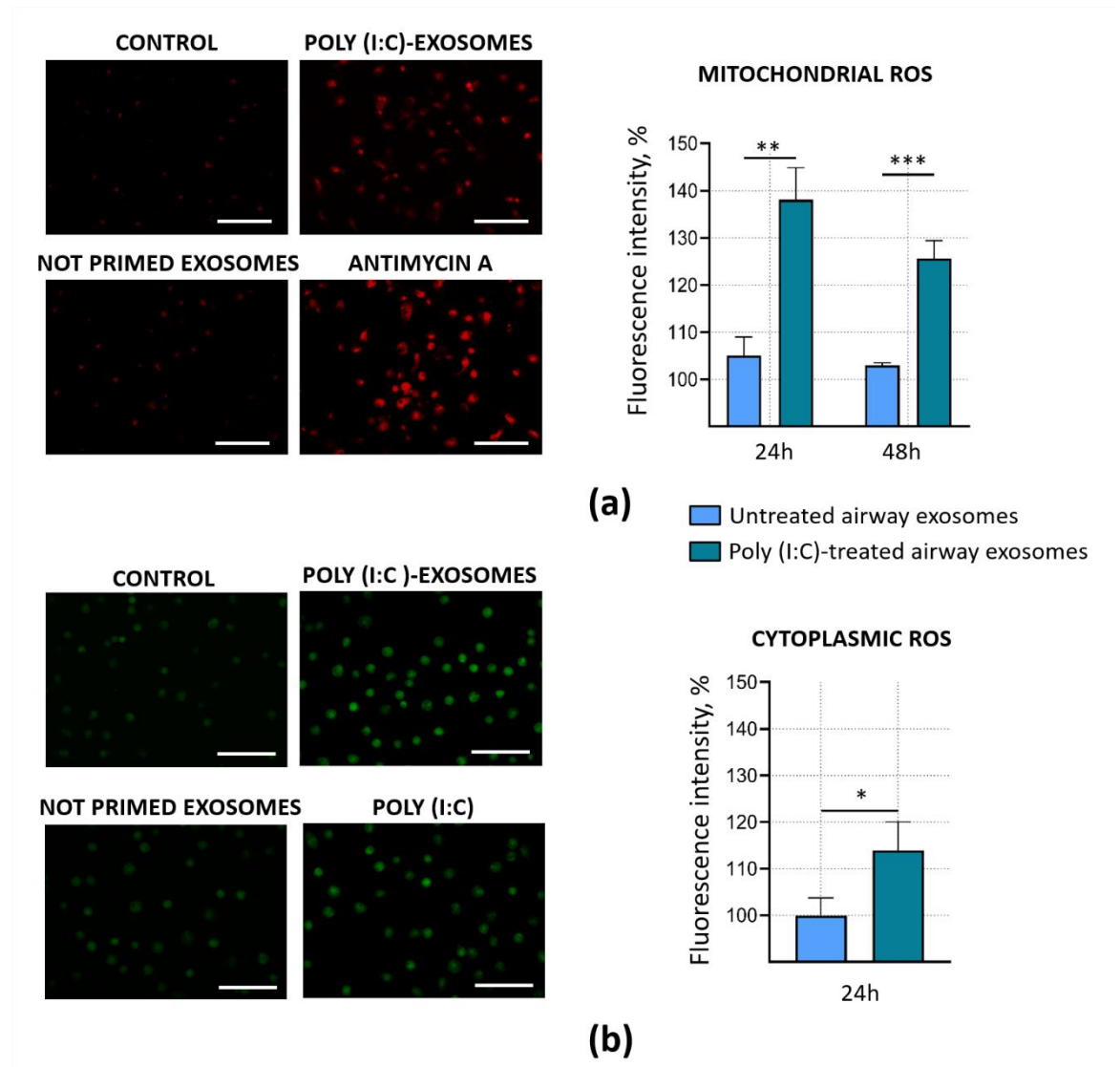

Figure 5. Intramitochondrial and cytoplasmic reactive oxygen species (ROS) formation in microglia after treatment with exosomes from poly (I:C)-primed airway cells. Cytoplasmic ROS were detected by DCFDA assay and mitochondrial superoxide – by MitoSOX™ fluorescence. (**a**) – representative images and quantitative evaluation of MitoSOX fluorescence in cultured microglia. For positive control of the assay, 100 µM Antimycin A was used. Scale bar is 100 µm. (**b**) – representative images and quantitative evaluation of 2,7-dichlorofluorescein (derived from DCFDA) fluorescence in microglial cultures. For positive control of the assay, 1 µg/mL poly (I:C) was used. Scale bar is 100 µm. The quantitative data of ROS-dependent fluorescence intensity in micrographs are presented as percentage of untreated control and expressed as averages ± standard deviation of 3 experiments in 3 biological replicates.   *** indicates statistically significant difference when $p < 0.001$; ** - $p < 0.01$; * - $p < 0.05$.

4. Discussion

The main highlights of the present study include confirmation that (1) airway cell exosomes easily penetrate the blood-brain barrier of healthy laboratory mice and (2) are quickly (within an hour or two) internalised by microglial cells. Moreover, (3) the exosomes from airway cells that received viral infection mimicking priming induce specific changes in microglial cells, leading to increased intracellular and intramitochondrial ROS generation.

Upper respiratory tract infections result in 10 million outpatient visits per year, and 70–90% of these infections are of viral origin [31,32]. Viral infections promote innate or non-specific and acquired or specific immune responses. There is a well-established correlation between peripheral viral infection and neuroinflammation that might lead to neurodegeneration [33,34]. The recently emerged SARS-CoV-2 virus that caused COVID-19 pandemia is also not an exception from this point of view; there are numerous reports about neuroinflammation-related central nervous system damage caused by this infection [35]. However, the mechanisms transmitting inflammation from the periphery to the brain remains elusive.

One of the most suggestable candidates for inflammation transmission from the periphery to the brain is exosomes. Exosomes of cells affected by bacteria, viruses, parasites, or fungi contain pathogen components that can be transferred to other cells [36]. Exosomes produced by bacterial infection-affected macrophages contain proinflammatory factors that activate B and T lymphocytes enhancing the immune response [37,38]. Virus-treated cells contain viral proteins and RNA that cause inflammatory response or even infection in recipient cells [36]. Herpes simplex, hepatitis A, B, C, and human immunodeficiency (HIV) viruses spread through exosomes [39–42]. The above-listed evidence allows assuming that some of the exosomes produced by infected cells could penetrate the central nervous system and cause neuroinflammation. Although several studies report peripheral exosomes crossing the blood-brain barrier [41,42], their further cellular uptake remained unknown. In addition, none of the examined exosomes originated from airway epithelium or fibroblasts. Our study experimentally demonstrated fast brain uptake of airway epithelial exosomes and provided evidence about their localisation in microglial cells. In addition, the *in vivo* data were supported by *in vitro* experimental proof of much faster exosome uptake performance by microglia compared to astrocytes. Although this is not direct evidence of airway infection spreading to the brain, the study gives a solid reason and background for studying this possibility. Interestingly, there were visually more airway cell exosomes in the pyramidal neuron area of the hippocampus after intranasal introduction. Hippocampal neurons are the primary target of Alzheimer's disease, and the cause of such selective damage to this area remains unknown. The fact that the hippocampus selectively collects peripheral exosomes carrying inflammatory mediators suggests a new hypothesis for Alzheimer's disease development. The hippocampus and olfactory regions are anatomically close; they are connected by memory formation networks and participate in glymphatic brain clearance [44,45]. Such anatomical and functional relations likely favour exosome transmission from the nasal cavity. Similarly to our findings, microglial localisation of intravenously injected fluorescently labelled exosomes was observed by Li and colleagues [43]. The authors have found that exosomes from serum of LPS-treated mice initiate inflammation in the brains of healthy exosome recipients. Such results strongly suggest that peripheral exosomes might be important yet underestimated players in neuroinflammation.

This study demonstrated that exosomes from virus mimetic-treated airway cells stimulate ROS generation in cultivated microglia. We have applied two different assays for ROS evaluation. Conversion of DCFDA to fluorescent 2,7-dichlorofluorescein (DCF) indicates hydroxyl, peroxyl and some other species produced into cell cytoplasm [46]. Mitochondrially targeted MitoSOX™ Red, in its turn, reports about the intensity of generation of superoxide radicals within mitochondria. Of all ROS, the respiratory chain primarily produces superoxide, which cannot cross membranes and remains where made unless converted to hydrogen peroxide by superoxide dismutase. Hydrogen peroxide molecules penetrate mitochondrial membranes to the cytosol, where it often undergoes further

conversions depending on the chemical environment, e.g., to hydroxyl radical by Fenton reaction. Thus, mitochondrial superoxide could also be the source of cytoplasmic ROS detected by the DCFDA reaction. The fact that poly (I:C)-primed airway exosomes stimulated mitochondrial superoxide generation far more intensively than intracellular (cytoplasmic) ROS strongly suggests mitochondria were the primary source of radicals in this case. However, to prove this hypothesis, more experimental evidence is required, such as testing how microglial cytoplasmic ROS levels induced by poly (I:C)-primed airway exosomes would be affected by the presence of mitochondrial superoxide scavenger mito-TEMPO.

Reactive oxygen species, including those from mitochondria, are generated as a fast response to infection [28,47]. Mitochondrial ROS lie at the top of the innate immune response cascade and precedes ROS generation from phagocytosis-related NADPH oxidase [48]. Moreover, they are required for virus-induced mitochondrial antiviral signalling protein (MAVS) to activate inflammasome [49,50], which is directly linked to neurodegeneration according to recent research [51,52]. Such an important role of mitochondrial ROS in inflammatory response indicate the following landmarks in dissecting the role of virus-primed airway cell exosomes, such as examining their effect on the mitochondrial and glycolytic profile of microglial cells inflammatory cytokine expression and secretion, inflammasome activation and impact on the inflammatory level in the brain. Also, elucidating the mechanism of exosome crossing the blood-brain barrier under the ordinary and infection-affected conditions and identifying the virus-induced molecular profile of airway cell exosomes would be of great importance in understanding the role of these extracellular vesicles in communication between the periphery and brain during viral infections.

5. Conclusions

- Virus mimetic poly (I:C)-primed and not primed airway cell exosomes reach brain tissue after not more than an hour from the intranasal introduction in mice.
- Both in the brain and culture, airway cell exosomes are internalised mainly by microglial cells.
- In pure microglial and mixed glial cultures, poly (I:C)-primed and not primed airway cell exosomes relocate from the extracellular medium to microglia within 30 min. During this period, the exosomes are not taken up by astrocytes.
- Airway exosome uptake does not influence the viability of microglial cells.
- Poly (I:C)-primed airway exosomes induce a significant and lasting increase in cytoplasmic and intramitochondrial ROS production. Conversely, the exosomes from not primed airway cells do not cause changes in ROS levels.

Author Contributions: Conceptualisation, L.J., R.M. and A.J.; methodology, D.K., L.J., N.P., Z.M., Z.B., and A.J.; formal analysis, D.K., O.J., L.J., H.I., and I.S.; investigation, D.K., D.N., O.J., L.J., A.M., N.P., J.S., H.I., Z.M. and I.S.; writing—original draft preparation, D.G. and A.J.; writing—review and editing, D.G., N.P., R.M., D.H.P. and A.J.; visualisation, D.K. and D.G.; supervision, D.H.P., R.M. and A.J. All authors have read and agreed to the published version of the manuscript.

Institutional Review Board Statement: The study was conducted according to the guidelines of the Declaration of Helsinki, and approved by the Lithuanian Food and Veterinary Service (protocol code G2-96, 2018, 14th of November).

Data Availability Statement: The raw data supporting the conclusions of this manuscript will be made available by the authors, without undue reservation, to any qualified researcher.

Conflicts of Interest: The authors declare no conflict of interest.

Appendix A

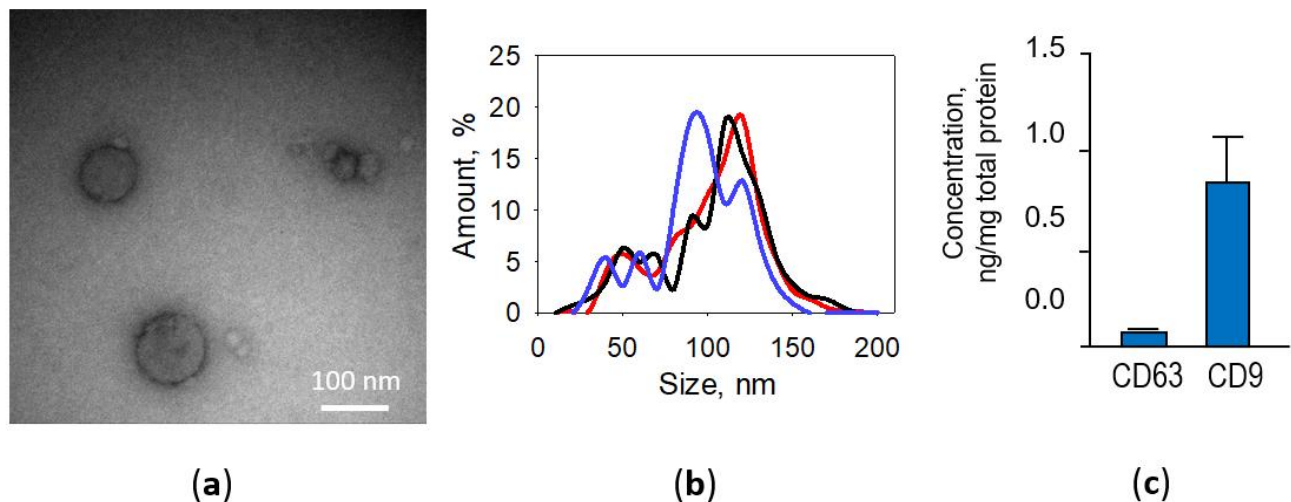**(a)**   **(b)**   **(c)**

Figure A1. Characterisation of mouse airway exosomes. A representative electron microscopy image (a), particle size and amount distribution (b), and evaluation of specific protein markers CD9 and CD63 (c).
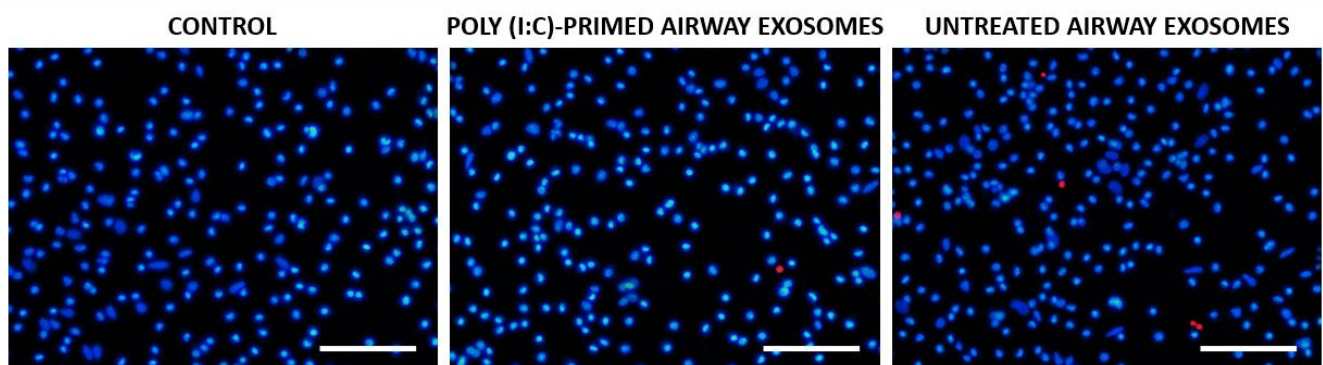

CONTROL   POLY (I:C)-PRIMED AIRWAY EXOSOMES   UNTREATED AIRWAY EXOSOMES

Figure A2. Representative images of viability evaluation of airway exosome-treated microglial cultures. The cells were stained with Hoechst33342 to visualise all nuclei blue and with propidium iodide to detect dying cells with lost plasma membrane integrity (red fluorescence of the nuclei).

References

1. Goody, M.F.; Sullivan, C.; Kim, C.H. Studying the immune response to human viral infections using zebrafish. *Dev. Comp. Immunol.* 2014, *46*, 84–95.
2. Mackie, P.L. The classification of viruses infecting the respiratory tract. *Paediatr. Respir. Rev.* 2003, *4*, 84–90.
3. Chahar, H.S.; Corsello, T.; Kudlicki, A.S.; Komaravelli, N.; Casola, A. Respiratory Syncytial Virus Infection Changes Cargo Composition of Exosome Released from Airway Epithelial Cells. *Sci. Rep.* **2018**, *8*, 387, doi:10.1038/s41598-017-18672-5.
4. Hassanpour, M.; Rezaie, J.; Nouri, M.; Panahi, Y. The role of extracellular vesicles in COVID-19 virus infection. *Infect. Genet. Evol.* 2020, *85*, 104422.
5. Gunasekaran, M.; Bansal, S.; Ravichandran, R.; Sharma, M.; Perincheri, S.; Rodriguez, F.; Hachem, R.; Fisher, C.E.; Limaye, A.P.; Omar, A.; et al. Respiratory viral infection in lung transplantation induces exosomes that trigger chronic rejection. *J. Hear. Lung Transplant.* **2020**, *39*, 379–388, doi:10.1016/j.healun.2019.12.009.
6. Zomer, A.; Vendrig, T.; Hopmans, E.S.; van Eijndhoven, M.; Middeldorp, J.M.; Pegtel, D.M. Exosomes. *Commun. Integr. Biol.* **2010**, *3*, 447–450, doi:10.4161/cib.3.5.12339.
7. Exosomes: biogenesis, biologic function and clinical potential Available online: https://www.ncbi.nlm.nih.gov/pmc/articles/PMC6377728/ (accessed on Feb 14, 2020).
8. Keerthikumar, S.; Chisanga, D.; Ariyaratne, D.; Al Saffar, H.; Anand, S.; Zhao, K.; Samuel, M.; Pathan, M.; Jois, M.; Chilamkurti, N.; et al. ExoCarta: A Web-Based Compendium of Exosomal Cargo. *J. Mol. Biol.* **2016**, *428*, 688–692, doi:10.1016/j.jmb.2015.09.019.

9.   Rajagopal, C.; Harikumar, K.B. The origin and functions of exosomes in cancer. *Front. Oncol.* 2018, *8*, 66.

10.   Xu, M.Y.; Ye, Z.S.; Song, X.T.; Huang, R.C. Differences in the cargos and functions of exosomes derived from six cardiac cell types: A systematic review. *Stem Cell Res. Ther.* 2019, *10*, 1–11.

11.   Flanagan, J.; Middeldorp, J.; Sculley, T. Localization of the Epstein-Barr virus protein LMP 1 to exosomes. *J. Gen. Virol.* **2003**, *84*, 1871–1879, doi:10.1099/vir.0.18944-0.

12.   Narayanan, A.; Iordanskiy, S.; Das, R.; Van Duyne, R.; Santos, S.; Jaworski, E.; Guendel, I.; Sampey, G.; Dalby, E.; Iglesias-Ussel, M.; et al. Exosomes derived from HIV-1-infected cells contain trans-activation response element RNA. *J. Biol. Chem.* **2013**, *288*, 20014–20033, doi:10.1074/jbc.M112.438895.

13.   Choi, H.; Lee, H.; Kim, S.R.; Gho, Y.S.; Lee, S.K. Epstein-Barr Virus-Encoded MicroRNA BART15-3p Promotes Cell Apoptosis Partially by Targeting BRUCE. *J. Virol.* **2013**, *87*, 8135–8144, doi:10.1128/jvi.03159-12.

14.   Pegtel, D.M.; Cosmopoulos, K.; Thorley-Lawson, D.A.; Van Eijndhoven, M.A.J.; Hopmans, E.S.; Lindenberg, J.L.; De Gruijl, T.D.; Würdinger, T.; Middeldorp, J.M. Functional delivery of viral miRNAs via exosomes. *Proc. Natl. Acad. Sci. U. S. A.* **2010**, *107*, 6328–6333, doi:10.1073/pnas.0914843107.

15.   Haneklaus, M.; Gerlic, M.; Kurowska-Stolarska, M.; Rainey, A.-A.; Pich, D.; McInnes, I.B.; Hammerschmidt, W.; O'Neill, L.A.J.; Masters, S.L. Cutting Edge: miR-223 and EBV miR-BART15 Regulate the NLRP3 Inflammasome and IL-1β Production. *J. Immunol.* **2012**, *189*, 3795–3799, doi:10.4049/jimmunol.1200312.

16.   Banks, W.A.; Sharma, P.; Bullock, K.M.; Hansen, K.M.; Ludwig, N.; Whiteside, T.L. Transport of extracellular vesicles across the blood-brain barrier: Brain pharmacokinetics and effects of inflammation. *Int. J. Mol. Sci.* **2020**, *21*, 1–21, doi:10.3390/ijms21124407.

17.   Alvarez-Erviti, L.; Seow, Y.; Yin, H.; Betts, C.; Lakhal, S.; Wood, M.J.A. Delivery of siRNA to the mouse brain by systemic injection of targeted exosomes. *Nat. Biotechnol.* **2011**, *29*, 341–345, doi:10.1038/nbt.1807.

18.   Li, Q.; Barres, B.A. Microglia and macrophages in brain homeostasis and disease. *Nat. Rev. Immunol.* 2018, *18*, 225–242.

19.   Aguzzi, A.; Barres, B.A.; Bennett, M.L. Microglia: Scapegoat, saboteur, or something else? *Science (80-.).* 2013, *339*, 156–161.

20.   Paolicelli, R.C.; Bolasco, G.; Pagani, F.; Maggi, L.; Scianni, M.; Panzanelli, P.; Giustetto, M.; Ferreira, T.A.; Guiducci, E.; Dumas, L.; et al. Synaptic pruning by microglia is necessary for normal brain development. *Science (80-.).* **2011**, *333*, 1456–1458, doi:10.1126/science.1202529.

21.   Fu, R.; Shen, Q.; Xu, P.; Luo, J.J.; Tang, Y. Phagocytosis of microglia in the central nervous system diseases. *Mol. Neurobiol.* **2014**, *49*, 1422–1434, doi:10.1007/s12035-013-8620-6.

22.   Brown, G.C.; Neher, J.J. Microglial phagocytosis of live neurons. *Nat. Rev. Neurosci.* **2014**, *15*, 209–216, doi:10.1038/nrn3710.

23.   Ransohoff, R.M. How neuroinflammation contributes to neurodegeneration. *Science (80-.).* 2016, *353*, 777–783.

24.   Wendeln, A.-C.; Degenhardt, K.; Kaurani, L.; Gertig, M.; Ulas, T.; Jain, G.; Wagner, J.; Häsler, L.M.; Wild, K.; Skodras, A.; et al. Innate immune memory in the brain shapes neurological disease hallmarks. *Nature* **2018**, *556*, 332–338, doi:10.1038/s41586-018-0023-4.

25.   Weinberg, S.E.; Sena, L.A.; Chandel, N.S. Mitochondria in the Regulation of Innate and Adaptive Immunity. *Immunity* **2015**, *42*, 406–417, doi:10.1016/j.immuni.2015.02.002.

26.   Balion, Z.; Cėpla, V.; Svirskiene, N.; Svirskis, G.; Druceikaitė, K.; Inokaitis, H.; Rusteikaitė, J.; Masilionis, I.; Stankevičienė, G.; Jelinskas, T.; et al. Cerebellar cells self-assemble into functional organoids on synthetic, chemically crosslinked ECM-mimicking peptide hydrogels. *Biomolecules* **2020**, *10*, 754, doi:10.3390/biom10050754.

27.   Dematteis, G.; Vydmantaitė, G.; Ruffinatti, F.A.; Chahin, M.; Farruggio, S.; Barberis, E.; Ferrari, E.; Marengo, E.; Distasi, C.; Morkūnienė, R.; et al. Proteomic analysis links alterations of bioenergetics, mitochondria-ER interactions and proteostasis in hippocampal astrocytes from 3xTg-AD mice. *Cell Death Dis.* **2020**, *11*, 1–16, doi:10.1038/s41419-020-02911-1.

28.   West, A.P.; Shadel, G.S.; Ghosh, S. Mitochondria in innate immune responses. *Nat. Rev. Immunol.* 2011, *11*, 389–402.

29.   Kim, H.J.; Kim, C.H.; Ryu, J.H.; Kim, M.J.; Park, C.Y.; Lee, J.M.; Holtzman, M.J.; Yoon, J.H. Reactive oxygen species induce antiviral innate immune response through IFN-λ regulation in human nasal epithelial cells. *Am. J. Respir. Cell Mol. Biol.* **2013**, *49*, 855–865, doi:10.1165/rcmb.2013-0003OC.

30.   Kim, S.; Kim, M.J.; Park, D.Y.; Chung, H.J.; Kim, C.H.; Yoon, J.H.; Kim, H.J. Mitochondrial reactive oxygen species modulate innate immune response to influenza A virus in human nasal epithelium. *Antiviral Res.* **2015**, *119*, 78–83, doi:10.1016/j.antiviral.2015.04.011.

31.   Meneghetti, A. Upper Respiratory Tract Infection Medication. *Medscape* **2015**, 1–18.

32.   Eugenia, M.; Patricia, D.; Horacio, L.; Ocadiz-Delgado, R.; Cabello-Gutierrez, C. Pathogenesis of Viral Respiratory Infection. In *Respiratory Disease and Infection - A New Insight*; InTech, 2013.

33.   Steel, A.J.; Eslick, G.D. Herpes viruses increase the risk of Alzheimer's disease: A meta-analysis. *J. Alzheimer's Dis.* **2015**, *47*, 351–364, doi:10.3233/JAD-140822.

34.   Klein, R.S.; Garber, C.; Funk, K.E.; Salimi, H.; Soung, A.; Kanmogne, M.; Manivasagam, S.; Agner, S.; Cain, M. Neuroinflammation During RNA Viral Infections. *Annu. Rev. Immunol.* 2019, *37*, 73–95.

35.   Amruta, N.; Chastain, W.H.; Paz, M.; Solch, R.J.; Murray-Brown, I.C.; Befeler, J.B.; Gressett, T.E.; Longo, M.T.; Engler-Chiurazzi, E.B.; Bix, G. SARS-CoV-2 mediated neuroinflammation and the impact of COVID-19 in neurological disorders. *Cytokine Growth Factor Rev.* 2021, *58*, 1–15.

36.   Schorey, J.S.; Cheng, Y.; Singh, P.P.; Smith, V.L. Exosomes and other extracellular vesicles in host–pathogen interactions. *EMBO Rep.* **2015**, *16*, 24–43, doi:10.15252/embr.201439363.

37. Quah, B.J.C.; O'Neill, H.C.   Mycoplasma contaminants present in exosome preparations induce polyclonal B cell responses . *J. Leukoc. Biol.* **2007**, *82*, 1070–1082, doi:10.1189/jlb.0507277.

38. Bhatnagar, S.; Schorey, J.S. Exosomes released from infected macrophages contain Mycobacterium avium glycopeptidolipids and are proinflammatory. *J. Biol. Chem.* **2007**, *282*, 25779–25789, doi:10.1074/jbc.M702277200.

39. Kulkarni, R.; Prasad, A. Exosomes Derived from HIV-1 Infected DCs Mediate Viral trans-Infection via Fibronectin and Galectin-3. *Sci. Rep.* **2017**, *7*, 1–14, doi:10.1038/s41598-017-14817-8.

40. Bello-Morales, R.; Praena, B.; de la Nuez, C.; Rejas, M.T.; Guerra, M.; Galán-Ganga, M.; Izquierdo, M.; Calvo, V.; Krummenacher, C.; López-Guerrero, J.A. Role of Microvesicles in the Spread of Herpes Simplex Virus 1 in Oligodendrocytic Cells. *J. Virol.* **2018**, *92*, 88–106, doi:10.1128/jvi.00088-18.

41. Lenassi, M.; Cagney, G.; Liao, M.; Vaupotič, T.; Bartholomeeusen, K.; Cheng, Y.; Krogan, N.J.; Plemenitaš, A.; Peterlin, B.M. HIV Nef is secreted in exosomes and triggers apoptosis in bystander CD4+ T cells. *Traffic* **2010**, *11*, 110–122, doi:10.1111/j.1600-0854.2009.01006.x.

42. Longatti, A. The dual role of exosomes in hepatitis A and C virus transmission and viral immune activation. *Viruses* 2015, *7*, 6707–6715.

43. Li, J.J.; Wang, B.; Kodali, M.C.; Chen, C.; Kim, E.; Patters, B.J.; Lan, L.; Kumar, S.; Wang, X.; Yue, J.; et al. In vivo evidence for the contribution of peripheral circulating inflammatory exosomes to neuroinflammation. *J. Neuroinflammation* **2018**, *15*, doi:10.1186/S12974-017-1038-8.

44. B, G.; LM, K.; C, M. Directional coupling from the olfactory bulb to the hippocampus during a go/no-go odor discrimination task. *J. Neurophysiol.* **2010**, *103*, 2633–2641, doi:10.1152/JN.01075.2009.

45. Natale, G.; Limanaqi, F.; Busceti, C.L.; Mastroiacovo, F.; Nicoletti, F.; Puglisi-Allegra, S.; Fornai, F. Glymphatic System as a Gateway to Connect Neurodegeneration From Periphery to CNS. *Front. Neurosci.* **2021**, *15*, 92, doi:10.3389/FNINS.2021.639140.

46. Dikalov, S.I.; Harrison, D.G. Methods for detection of mitochondrial and cellular reactive oxygen species. *Antioxidants Redox Signal.* 2014, *20*, 372–382.

47. Bulua, A.C.; Simon, A.; Maddipati, R.; Pelletier, M.; Park, H.; Kim, K.Y.; Sack, M.N.; Kastner, D.L.; Siegel, R.M. Mitochondrial reactive oxygen species promote production of proinflammatory cytokines and are elevated in TNFR1-associated periodic syndrome (TRAPS). *J. Exp. Med.* **2011**, *208*, 519–533, doi:10.1084/jem.20102049.

48. Chen, Y.; Zhou, Z.; Min, W. Mitochondria, oxidative stress and innate immunity. *Front. Physiol.* 2018, *9*, 1487.

49. Subramanian, N.; Natarajan, K.; Clatworthy, M.R.; Wang, Z.; Germain, R.N. The adaptor MAVS promotes NLRP3 mitochondrial localisation and inflammasome activation. *Cell* **2013**, *153*, 348–361, doi:10.1016/j.cell.2013.02.054.

50. Onomoto, K.; Onoguchi, K.; Yoneyama, M. Regulation of RIG-I-like receptor-mediated signaling: interaction between host and viral factors. *Cell. Mol. Immunol.* 2021, *18*, 539–555.

51. Heneka, M.T.; Kummer, M.P.; Stutz, A.; Delekate, A.; Schwartz, S.; Vieira-Saecker, A.; Griep, A.; Axt, D.; Remus, A.; Tzeng, T.C.; et al. NLRP3 is activated in Alzheimer's disease and contributes to pathology in APP/PS1 mice. *Nature* **2013**, *493*, 674–678, doi:10.1038/nature11729.

52. Lee, E.; Hwang, I.; Park, S.; Hong, S.; Hwang, B.; Cho, Y.; Son, J.; Yu, J.W. MPTP-driven NLRP3 inflammasome activation in microglia plays a central role in dopaminergic neurodegeneration. *Cell Death Differ.* **2019**, *26*, 213–228, doi:10.1038/s41418-018-0124-5.